Energy & Environmental Science

PAPER

View Article Online
View Journal | View Issue

Tuning bands of PbSe for better thermoelectric efficiency†

Cite this: *Energy Environ. Sci.*, 2014, **7**, 804

Heng Wang,*[a] Zachary M. Gibbs,[b] Yoshiki Takagiwa[c] and G. Jeffrey Snyder*[a]

Received 16th October 2013
Accepted 26th November 2013

DOI: 10.1039/c3ee43438a

www.rsc.org/ees

Improving the thermoelectric performance of PbSe over its previously reported maximum zT can be achieved by engineering its electronic band structure. We demonstrate here, using optical absorption spectra, first principles calculations, and temperature dependent transport measurements, that alloying PbSe with SrSe leads to a dramatic change of the band structure that increases the thermoelectric figure of merit, zT. The temperature where the two valence bands converge decreases with Sr addition. The zT value, when the carrier density is optimized, increases with Sr addition in $Pb_{1-x}Sr_xSe$ and when $x = 0.08$ a maximum zT of 1.5 at 900 K is achieved. The net benefit in zT comes from the band structure tuning even though in other thermoelectric solid solutions it is the thermal conductivity reduction from disorder that leads to net zT improvement.

Broader context

Band engineering in semiconductors is important for their application in electronic or optoelectronic devices. For heavily doped thermoelectric semiconductors it is also crucial for the high zT found in $PbTe_{1-x}Se_x$, $Pb_{1-x}Mg_xTe$, and $Mg_2Si_{1-x}Sn_x$. For high temperature bulk thermoelectrics, most of such engineering is realized by forming solid solutions. In this study we demonstrate successful band tuning of p-type PbSe, the slightly lower zT analog of the well-known thermoelectric compound PbTe, using $Pb_{1-x}Sr_xSe$ solid solutions. It is well known that formation of solid solutions is desirable for thermoelectrics due to their lower thermal conductivities. We demonstrate here that the ability to change not only the band gap but also the relative positions of different band maxima provides another important benefit for solid solutions as thermoelectrics. Actually, we found in these alloys that the reduction of lattice thermal conductivity by alloying has been compensated by the counter effect of the reduced carrier mobility, as also been found in the n-type solid solutions $PbTe_{1-x}Se_x$ and $PbSe_{1-x}S_x$ where simply forming solid solutions without the band engineering effect does not improve zT. Therefore we conclude that the change in the band structure with formation of solid solution accounts for the improvement of zT in p-type PbSe from 1.1 to 1.5 at 900 K.

Introduction

PbSe is a promising thermoelectric material[1] that does not rely on the scarce element Te. The thermoelectric figure of merit $zT = S^2\sigma T/(\kappa_e + \kappa_L)$ (S is the Seebeck coefficient, σ is the electric conductivity, and κ_e and κ_L are the electronic and lattice thermal conductivity, respectively) for both n-type[2–4] and p-type[5–7] PbSe exceeds 1 at high temperature. Although similar to its well-studied analog PbTe,[8–10] PbSe has an easily recognizable difference in the band structure[11–14] leading to different transport behavior and lower maximum zT. Nonetheless, we demonstrate here, using PbSe alloyed with SrSe, that by tuning its valence band structure the good zT found in p-type PbSe could be further enhanced. The introduction of Sr makes the contribution from the secondary, multi-valley valence band to carrier transport greater over a broader temperature range so a maximum zT of 1.5 at 900 K is obtained. The high zT comes from the change in the valence band structure rather than the atomic disorder that commonly benefits zT in thermoelectric solid solutions.[15] Band engineering is another important facet in addition to the historic motivation of forming solid solution in thermoelectrics.

In PbSe as well as PbTe, the secondary valence band maximum (along the Σ line of the Brillouin zone, called the Σ band) contributes to the carrier transport at high temperature when the energy of the primary valence band (the L band) decreases as the band gap increases with temperature.[11,16–18] The best thermoelectric performance is found around temperatures where the two valence bands are converged (within a few k_BT of one another).[19,20] For PbTe the convergence temperature (T_{cvg}) was believed to be around 450 K based on both optical band gap measurements[16,18] and temperature dependent Hall coefficient data.[19,21,22] However, new evidence and data interpretation[23,24] have indicated that the

[a]*Materials Science, California Institute of Technology, Pasadena, CA 91125, USA. E-mail: hengwang@caltech.edu; jsnyder@caltech.edu*

[b]*Chemistry and Chemical Engineering, California Institute of Technology, Pasadena, CA 91125, USA*

[c]*Department of Advanced Materials Science, The University of Tokyo, Kiban-toh 502, 5-1-5 Kashiwanoha, Kashiwa-shi, Chiba 277-8561, Japan*

† Electronic supplementary information (ESI) available: (1) XRD and absorption spectrum. (2) Temperature dependent transport properties for all samples studied. (3) Calculation details of the Pisarenko relation for $Pb_{1-x}Sr_xSe$ samples. (4) Calculation of lattice thermal conductivity from a point defect model for alloys. (5) Calculation of alloy scattering potential from undoped samples. See DOI: 10.1039/c3ee43438a

actual convergence temperature should be higher. In PbSe, the Σ band is further away[25,26] (~0.3 eV at 0 K) from the primary band maximum and the two bands converge at a higher temperature. Early studies[11,25,27,28] based on Hall coefficient data have pointed to a T_{cvg} of around 750 K. However, the result based on optical absorption spectra[24,29] (for T below 500 K) suggests that this temperature in PbSe should be around 900–1100 K, which is beyond the highest feasible operating temperature for PbSe. Bringing this temperature down to, for instance, 800 K by tuning up the valence band structure of PbSe would potentially improve the thermoelectric performance of p-type PbSe.

There are two strategies for reducing the convergence temperature in PbSe: the first strategy is alloying PbSe with PbTe. Being analogous to the effect seen in PbTe rich $PbTe_{1-x}Se_x$ alloys,[19] the addition of PbTe into PbSe would make the valence bands more PbTe-like therefore lower T_{cvg}. Two drawbacks can be anticipated for this strategy: first, an excessive degree of alloying will be needed due to the small difference in band structures (50% PbTe addition estimated to bring T_{cvg} down to 800 K). Second, the disorder introduced by Te substitution of Se in PbSe is not thermoelectrically beneficial.[15]

The other strategy is alloying PbSe with alkaline-earth selenides that are of rock-salt structures and wide band gaps. No report on phase diagrams between PbSe and MSe (M = Mg, Ca, Sr, Ba) can be found. Thus, it is still unknown if such an alloy is thermodynamically stable in the bulk, or what effect alloying has on the band structure and transport properties. However, Molecular Beam Epitaxy (MBE) grown $Pb_{1-x}Sr_xSe$ thin films have been studied; they show that the lattice constant changes gradually following Vegard's law and the band gap tunable in a wide range with different SrSe contents.[30–32] Given the rock-salt structure and the lattice parameter[31] of 6.25 Å for SrSe it is highly probable that an appreciable solubility of SrSe in PbSe in the bulk could be found. On the other hand, recent studies on thermoelectric PbTe with SrTe addition implied that SrTe leads to noticeable thermal conductivity reduction without significantly impairing the carrier mobility,[33,34] which means the disorder might be beneficial in $Pb_{1-x}Sr_xSe$ alloys as well.

In this work we present the study of bulk $Pb_{1-x}Sr_xSe$ alloys with different 'x' up to 12%. For each alloy composition p-type dopant Na (K for two samples) is used to tune the carrier density and multiple doping levels are studied. Our result demonstrates that PbSe and SrSe form thermodynamically stable solid solutions in bulk form and the solubility of SrSe in PbSe is no less than 8%. The effect of Sr on the band structure is revealed by transport as well as optical absorption edge measurements. The band structure is sensitive to and gradually tunable with a small amount of Sr. An appreciable enhancement in thermoelectric performance was achieved and the maximum zT of 1.5 is found at 900 K (1.4 ± 0.1 in multiple samples with different compositions). Analysis further suggests that such an enhancement is purely due to the change of the band structure whereas the thermal conductivity reduction due to the disorder introduced from substituting Pb with Sr in PbSe is entirely compensated by the reduction in charge carrier mobility.

A similar study[35] of PbSe with alkaline-earth elements added was recently reported by Lee *et al.*, where the improvement of zT is believed to be due to the multi-scale hierarchical microstructure that reduced the lattice thermal conductivity, which is similar to the mechanism reported in the PbTe–SrTe system.[34] Most of the transport properties at high temperatures reported by Lee *et al.* are found to be consistent with our result, however, here we present a more comprehensive and extended study and propose an alternate explanation based on the change of the electronic band structure.

Results and discussion

All samples are single phase when characterized by X-ray diffraction (ESI†). The lattice constants increase with Sr content following the Vegard's law through 12% using a reported lattice constant[31] of 6.25 Å for SrSe (Fig. 1a). Scanning electron microscopy (SEM) on polished surfaces reveals a typical solid solution microstructure and no well dispersed secondary-phase precipitates down to 50 nm in size could be seen (Fig. 1b). The samples are also homogeneous on a large scale (100 μm) with no Sr segregation seen up to 8% Sr. Large Sr-rich inclusions (~10 μm in size) are only found in 12% Sr alloy with >10 μm intervals (Fig. 1c and d): a length scale well beyond the mean free path of charge carriers or phonons. The inhomogeneity usually suggests a solubility limit, but here could more likely be due to insufficient mixing of Sr and slow diffusion across some of the grain boundaries.

The optical band gaps of undoped $Pb_{1-x}Sr_xSe$ alloys are noticeably larger than those of PbSe (Fig. 2a). The band gap increases linearly with Sr content through 12% and is roughly doubled at this Sr content. For all alloys the absorption spectra are consistent with direct transitions and are attributed to L–L transitions as in pure PbSe.[26]

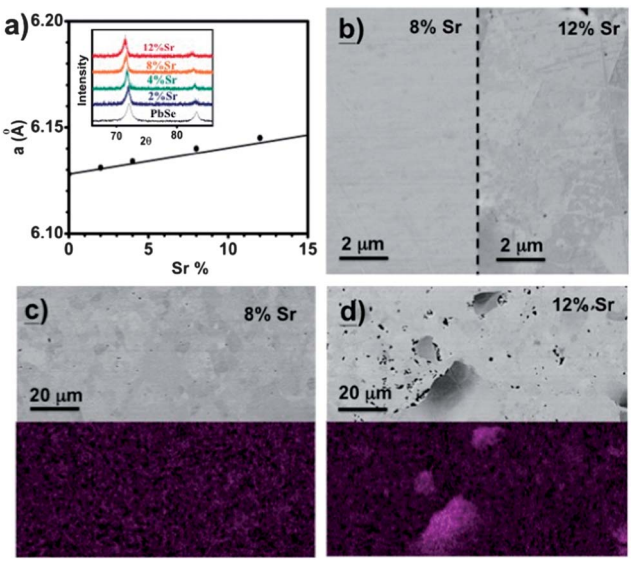

Fig. 1 (a) Lattice constant of $Pb_{1-x}Sr_xSe$ alloys following the Vegard's law (solid line), the inset shows the high angle peak shift without broadening. (b) SEM backscattered images of $Pb_{0.92}Sr_{0.08}Se$ and $Pb_{0.88}Sr_{0.12}Se$ ingots, no secondary phase inclusion is found at this scale for both. (c) Backscattered image of $Pb_{0.92}Sr_{0.08}Se$ at a large scale and the corresponding Sr EDS mapping result. (d) Backscattered image of $Pb_{0.88}Sr_{0.12}Se$ at a large scale and the Sr mapping result.

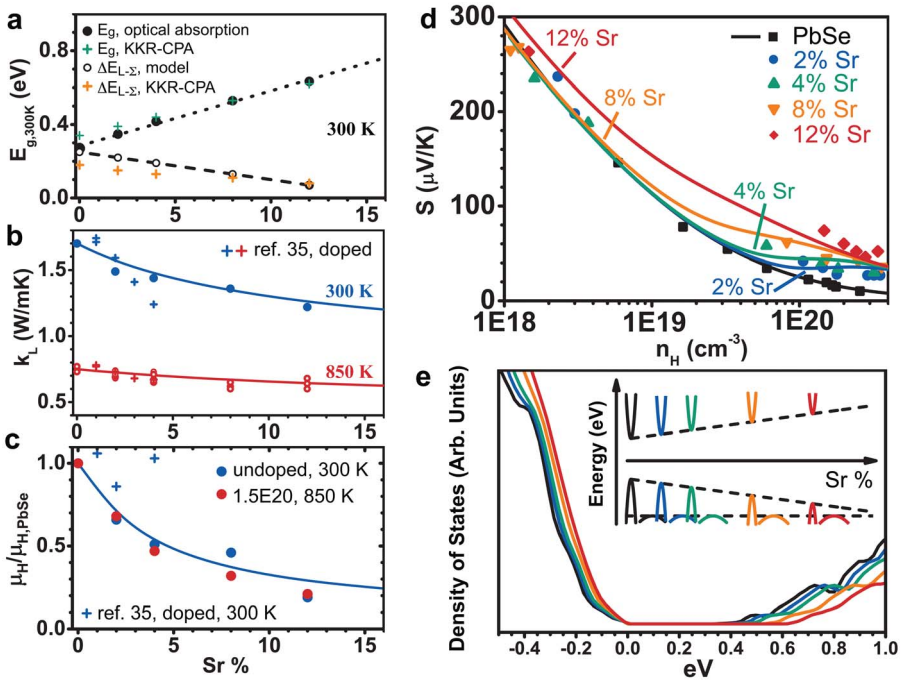

Fig. 2 (a) The measured band gap E_g and the proposed energy separation between two valence bands $\Delta E_{L-\Sigma}$ of $Pb_{1-x}Sr_xSe$ alloys, each is consistent with calculated values. (b) Lattice thermal conductivity as a function of Sr content at 300 K and 850 K. The 300 K values are from undoped samples. (c) Normalized Hall mobility as a function of Sr content for undoped samples at 300 K and doped samples with the same carrier density at 850 K. (d) Pisarenko relation of p-type PbSe and $Pb_{1-x}Sr_xSe$ alloys. Lines are calculated using the proposed band model. (e) The calculated DOS spectrum of $Pb_{1-x}Sr_xSe$ alloys and the inset illustrates the proposed band model, based on (a).

The change of the band structure consequently affects the transport properties. Fig. 2d shows the measured room temperature Seebeck coefficient as a function of Hall carrier density (the Pisarenko relation). For PbSe, due to the large offset between two valence-band maxima at room temperature, the contribution from the secondary Σ band to transport is negligible and the Pisarenko relation (data in black squares) can be explained with a single band model[2,36] (black curve) using parameters determined previously[2] for the L band. With the addition of Sr, the Seebeck coefficients start to deviate from the curve significantly at high doping levels, with higher values compared to PbSe given the same carrier density. Among the $Pb_{1-x}Sr_xSe$ alloys the Seebeck coefficient also increases as the Sr content increases. If the increased Seebeck values were simply due to a larger effective mass, the Seebeck value would be proportionally larger at all n_H, which is not observed in $Pb_{1-x}Sr_xSe$ alloys with low n_H. Alternatively the deviation from a single band model (the black curve) at high n_H indicates that the contribution from a second band becomes important as the Fermi level moves into the second valence band, which is also the explanation for the similar Pisarenko behavior in p-type PbTe.[8] The continuous change in the direct L–L band gap due to SrSe alloying can explain the gradual change of Pisarenko relation. If the energy of the L valence band is reduced as the band gap increases, which reduces the band offset in PbSe between L and Σ valence bands, the secondary Σ band will play a noticeable role in heavily doped, Sr containing PbSe.

We assume that the Σ band remains stationary while the L (conduction and valence) bands move apart, resulting in an energy separation between L and Σ valence bands that changes as roughly half of the band gap changes with Sr content (Fig. 2e), as inspired by observation[32] on thin films at 77 K, the calculated Pisarenko relations for each $Pb_{1-x}Sr_xSe$ alloy composition are shown in Fig. 2d with colored lines, and are in reasonable agreement with the observed results (see ESI† for calculation details).

Optical absorptions in the lead chalcogenides begin with direct transitions across the fundamental gap at the L point. Because these direct transitions do not require phonon participation, they dominate the absorption spectra compared with the L–Σ indirect transitions, which should occur at higher energies. This limits traditional optical absorption to accurately determine the position of the Σ band edge. Historically Russian scientists have used optical transition between two valence bands to derive the position of the Σ band edge.[25,29,37] This method to us is subject to interpretation and is prone to uncertainty in the free carrier absorption fit.

For more independent evidence of how the band structure changes with Sr content, we performed first principle calculation using the Korringa–Kohn–Rostoker Green function formalism under the coherent potential approximation[38–40] (KKR-CPA). The KKR-CPA method is a powerful tool for visualizing the electronic density of states (DOS) for disordered materials without establishing a supercell and is widely used in the studies of thermoelectrics with random substitution.[41–45]

Calculated DOS spectra of $Pb_{1-x}Sr_xSe$ confirmed both the increase of band gap and the decrease of energy separation between L and Σ bands. These are shown in Fig. 2a and are in good agreement with the proposed model.

In Fig. 3 the temperature dependent transport properties of $Pb_{1-x}Sr_xSe$ alloys with different Sr contents are compared. The samples shown have similar Hall carrier densities at room temperature of between 1.3 and 1.8 × 10^{20} cm^{-3} (properties of all samples studied, with different carrier densities for each Sr content, are shown in the ESI†). Na and K do not change the band structure of lead chalcogenides[41] and transport properties of Na and K doped samples are comparable when carrier density is similar (ESI†) thus all the difference shown in Fig. 3 is due to different Sr contents. The resistivity increases significantly with Sr content, which can be expected from increased alloy scattering of carriers. The increased resistivity also stems from the increased contribution from the Σ band that has a heavier effective mass. Compared with samples with same Sr content from this study, PbSe with 0%, 2% and 4% SrSe in ref. 35 each have very similar resistivities at high temperatures.

As shown in Fig. 3b alloys with higher Sr content have higher Seebeck coefficients. This trend is observed through the entire temperature range up to 8% Sr. The higher S values can be explained by the carrier redistribution between two valence bands, which populates more states in the high density-of-states Σ band in alloys with more Sr, so for a given carrier density the alloys with higher Sr content have more carriers in the Σ band hence the chemical potential is closer to the band edge. The alloy with 12% Sr shows higher S values compared with the 8% Sr alloy mainly around room temperature. This can be understood considering that as the T_{cvg} decreases the Σ band plays an increasingly important role in transport at high temperature in both 8% and 12% alloys thus the difference in chemical potential between them is small. The increase of S with Sr content was not as recognizable in Lee's work[35] where the difference between samples with 2% Sr and 4% Sr is comparable with measurement uncertainty, even though for each sample the result is generally consistent with this study (Fig. 3b).

The temperature dependence of the Hall coefficient (R_H) of each sample is compared in Fig. 3c. The relative ratios to their room temperature values are presented. In single-band systems the temperature dependence of R_H is weak and monotonic (see R_H for n-type PbS with $n_H = 1.2 \times 10^{20}$ cm^{-3} shown in Fig. 3c). Non-monotonic R_H–T curves usually indicate two types of carriers (electrons and holes, or electrons/holes with different effective masses) co-existing in transport,[19,29,46] and R_H peaks when the contribution from each type of carriers to conduction is equal[47] (such that T_{cvg} should be higher than the temperature where R_H peaks). Given their similar carrier density the difference in temperature where R_H peaks among different samples are primarily caused by the difference in the band structure: lower peaking temperature indicates more contribution from the secondary Σ band at a given temperature, which is the outcome of the reduced energy offset between L and Σ bands.

The thermal conductivities of $Pb_{1-x}Sr_xSe$ alloys are lower than those of PbSe (Fig. 3d). Compared with the values reported[35] by Lee *et al.*, thermal conductivities of $Pb_{1-x}Sr_xSe$ alloys in this work are found lower near room temperature due to larger resistivities. At high temperatures the results for the same alloy composition from both studies are found to be very similar.

Fig. 4 shows the maximum zT of different $Pb_{1-x}Sr_xSe$ alloys compared with that of PbSe (see ESI† for zT of each alloy composition with different carrier densities). The previously

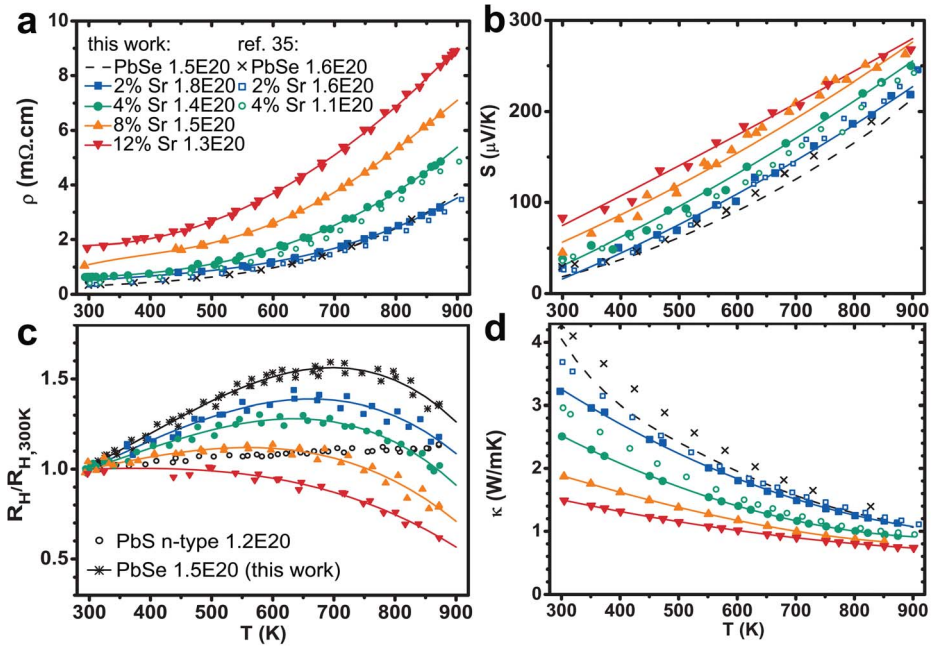

Fig. 3 The temperature dependence of transport properties: (a) resistivity, (b) Seebeck coefficient, (c) Hall coefficient and (d) thermal conductivity of $Pb_{1-x}Sr_xSe$ alloys. Numbers in (a) denotes the measured Hall carrier density at 300 K.

reported zT of 1.2 at 850 K for p-type PbSe,[5] which although has been reproduced by other researchers,[6,7] is reevaluated here to be 1.1 at 900 K (1.0 at 850 K). This value agrees with Lee's recent report[35] and is believed at this time to be most accurate (Fig. 3). Compared with PbSe, a noticeable improvement of zT is seen in $Pb_{1-x}Sr_xSe$ alloys for the Sr content as low as 2%: both this study and the recent report[35] have measured a zT of 1.3 at 900 K. The result from this study also indicates that zT can be further improved as the Sr content increases, a zT of 1.5 is observed at 900 K for properly doped alloy with 8% Sr, further increasing Sr content seems to reduce the maximum zT. The zT of 1.4 ± 0.1 at 900 K was achieved in multiple samples with different Sr contents, each requiring different carrier densities. As shown in Fig. 4 more carriers are required for alloys with higher Sr content, as the density-of-state effective mass increases with increased contribution from the Σ band.

Beside changing the band structure, the substitution of Sr on the Pb site also creates disorder and has its influence on zT by reducing the lattice thermal conductivity and carrier mobility, as shown in Fig. 2b and c.

In Fig. 2b, κ_L of alloys with different Sr contents at both 300 K and 850 K are compared (see ESI† for general temperature dependent κ_L). The 300 K data from this work are taken from undoped samples with high electrical resistivity and therefore negligible κ_e. κ_L at 850 K are evaluated with Lorenz number L from a single parabolic band model from doped samples. The thermal conductivity reduction in $Pb_{1-x}Sr_xSe$ alloys, which is more effective at room temperature and less so at 850 K, can be well explained by Callaway and Klemens' model[15,48–53] of thermal conductivity for alloy systems (the solid curves, see ESI† for detail). For 10% Sr as an example the κ_L reduction is 25% at 300 K, and 15% at 850 K as suggested by both the experimental trend and the model. At high temperature, κ_L from Lee's work[35] is found to follow the same trend. Differences can be seen at room temperature where larger reduction of κ_L (calculated from heavily doped samples) with Sr content has been reported.[35]

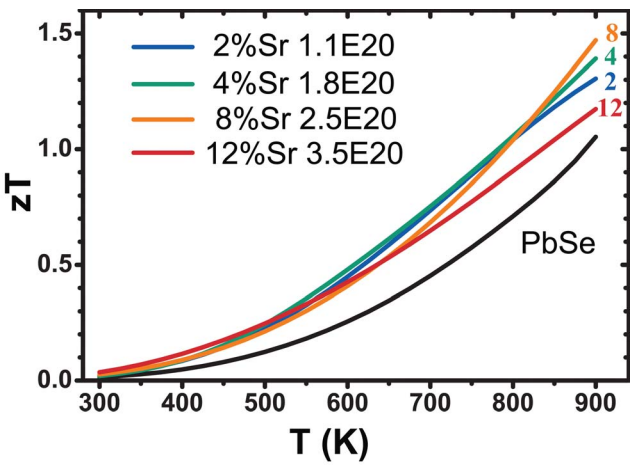

Fig. 4 The observed zT of samples that have highest zT at 900 K and the corresponding Hall carrier densities at room temperature for $Pb_{1-x}Sr_xSe$ with different Sr contents, compared to the maximum zT evaluated for p-type PbSe (zT for samples with different carrier densities at each Sr content shown in ESI†).

The Sr addition is also found to reduce the carrier mobility. In undoped samples the mobility reduction is solely related to the alloy scattering because the contribution from the secondary band is minimal and the effective mass of the L valence band stays unchanged in Sr alloys as in PbSe. For the mobility reduction in undoped $Pb_{1-x}Sr_xSe$ alloys ($n_{H,300K} \leq 3 \times 10^{18}$ cm^{-3}) at 300 K (expressed as measured Hall mobility relative to Hall mobility of PbSe with the same carrier density), the observed trend can be understood with alloy scattering[15,54–56] of carriers in addition to the deformation potential scattering within the framework of a single band model (see ESI† for detail). The magnitude of alloy scattering in the L valence band can thus be modeled (solid curve). The alloy scattering potential U, which measures the significance of alloy scattering, is estimated to be 3 eV for the L band. This is a fairly large U value compared to those reported for other systems.[15]

Being different from the undoped samples at 300 K, mobility reduction in heavily doped samples is the result of intertwined influence of alloy scattering and carrier re-distribution associated with the change of the valence band offset. Nonetheless in Fig. 2c the normalized mobilities at 850 K for samples with a similar carrier density around 1.5×10^{20} cm^{-3} are also shown. It provides a straightforward illustration, together with the reduction of κ_L in Fig. 2b, that the atomic disorder has induced more mobility reduction than thermal conductivity reduction, both at 300 K and 850 K.

The mobility of doped samples ($n_{H,300K} > 1 \times 10^{20}$ cm^{-3}) at 300 K was found in Lee's work[35] to not decrease with Sr addition relative to PbSe, similar to the previously suggested absence of mobility reduction[33] in Sr added PbTe. Despite the difference at room temperature in lattice thermal conductivity and Hall mobility between this study and Lee's report, the measured electrical resistivity and κ_L at high temperatures are very similar, as shown in Fig. 2b and 3a and d.

In a relevant case, the substitution of Se by Te has overall compensated effects[15] for n-type PbSe. For instance, 10% Te substitution resulted in roughly 20% decrease at 300 K in both lattice thermal conductivity and carrier mobility. As for $Pb_{1-x}Sr_xSe$, the κ_L reduction is higher at 25% for 10% Sr substitution, but the mobility suppression is much worse, down to <50%. The slightly larger κ_L reduction comes from larger mass contrast between Sr and Pb (compared with that between Se and Te). The much larger alloy scattering potential U (U around 1 eV for n-type $PbSe_{1-x}Te_x$) is probably linked to the larger mismatch of valence band energy: the electron affinity of SrSe is[57] 1.8 eV and its band gap (Γ–X) is[58,59] 3.8 eV, the top of its valence band at Γ point is thus 5.6 eV below the vacuum level. On the other hand the work function of PbSe is[60] 4.6 eV and the band gap 0.3 eV, which means the top of its L valence band is 4.8 eV below the vacuum level: a 0.8 eV difference in band energy between PbSe and SrSe. For comparison, the difference in conduction band energy between PbSe and PbTe is only[61] 0.1 eV.

The substitution of Pb by Sr in PbSe is thus an undesired disorder for thermoelectrics. Nonetheless, zT improvement is still achieved in $Pb_{1-x}Sr_xSe$ alloys because the valence band structures are tuned in favor of thermoelectric properties. Specifically, the gap between the primary L band and the

secondary Σ band is decreased, so that the highly degenerate Σ band could contribute more to the carrier transport. This effect, in $Pb_{1-x}Sr_xSe$, competes with the undesirable Pb site disorder. The net result is a significant increase of zT over a broad range of Sr content from 2% to 8%. When the Sr content is further increased, the negative effect of the Pb site disorder overwhelms resulting in decreased zT.

Conclusions

In summary, tuning the energy of the valence bands in PbSe has improved the thermoelectric properties of p-type PbSe over its already promising ones. Higher zT originates from a decreased energy offset between the primary and secondary valence bands and hence the decreased convergence temperature T_{cvg}. This effect is not restricted to $Pb_{1-x}Sr_xSe$: for instance other iso-valent selenides with a similar symmetry and band structure can be as effective, and Lee's result[35] has shown the merit of this strategy. If an element could be found where the right combination of mass contrast and valence band mismatch is found so that random alloying is thermoelectrically beneficial, the strategy of band engineering would work together with beneficial disorder to produce even higher zT. Moreover, this work suggests a promising route for increasing performance in other, less competitive thermoelectric materials that have similar valence band structures (PbS, SnTe). The similar chemistry between $Pb_{1-x}Sr_xSe$ and alkaline-earth added PbTe ($Pb_{1-x}Sr_xTe$[33,34] and $Pb_{1-x}Mg_xTe$[62,63]) implies that the improved thermoelectric performance in those systems could also originate from a similar effect that involves an increase of the contribution from the Σ band at different temperatures.

Experimental method

The samples are made *via* a conventional melting and pressing route. Undoped samples in 25 g batches were first made. To do so high purity elements (Pb, 99.999%; Se, 99.999%; Sr, 99.9%) were loaded and sealed in carbon coated quartz ampoules, then quickly melted for 15 minutes by induction heating. Each ingot was ground and hot pressed, then sealed in another ampoule and annealed at 1073 K for 14 days. The doped samples of each alloy composition was made by reacting powder (3 g) of undoped alloy with Na and Se at 1200 K for 5 days in sealed ampoules, and then hot pressed at 923 K. The disk samples for tests were 12.7 mm in diameter and about 1 mm thick with density no less than 97% of theoretical value.

Absorption edge measurements were carried out on undoped samples using a Nicolet 6700 FTIR Spectrophotometer equipped with a Praying Mantis Diffuse Reflectance attachment (Harrick Scientific Instruments) at 300 K. Measurements[64] were performed under an argon atmosphere. The scans were referenced to KBr standard samples. Optical gaps were extracted using the Tauc method where α was extrapolated to zero as a function of $(\hbar\omega)^n$. Here α is the absorption coefficient (whose proportionality was calculated using the Kubelka Munk function), $\hbar\omega$ is the incoming photon energy, and n is equal to 2 for direct gaps. Urbach tails (exponential increase in absorption) were observed but insignificant since the samples are undoped and thus were not subtracted for the Tauc fit.

For KKR-CPA calculation the experimental room-temperature lattice constants and the von Barth–Hedin formula[65] for the exchange energy were used. For all atoms (Pb, Se, and Sr), the angular momentum cut-off, $l_{max} = 2$, was set and semi-relativistic calculations of the core level were employed. A dense mesh of 550 k points in the irreducible wedge of the Brillouin-zone was used. Final converged total energy below 10^{-6} Ry was applied in the self-consistent cycle. The calculated DOS for each composition shows an abrupt increase around −0.1 eV, which is attributed to the additional states in the Σ band and its position is used to estimate the gap between L and Σ bands.

The in-plane resistivities and Hall coefficients (R_H) were measured using the Van der Pauw method[66] in a magnetic field up to ±2 T. The Seebeck coefficients were measured along the cross-plane direction using Chromel–Nb thermocouples.[67] The thermal conductivities were calculated from $\kappa = dD_TC_p$, with the thermal diffusivity D_T measured along the cross-plane direction by the laser flash method (Netzsch LFA 457) under argon flow with the Cowan model plus pulse correction. The heat capacity C_p was determined using the equation C_p/k_B per atom = 3.07 + 4.7 × 10^{-4} (T/K-300) by fitting experimental data.[68] All properties are isotropic based on our previous study of PbSe.[2] The result of each measurement was compared with those from different institutes on the same sample and is found very consistent.[2,65] For each measurement data were collected during both heating and cooling. The uncertainty of each measurement is about 5% which combined could lead to a maximum of 20% uncertainty in the zT value.

Acknowledgements

H. W., Z. M. G., and G. J. S. would like to thank AFOSR MURI FA9550-10-1-0533 and NASA/JPL for funding, and the Molecular Materials Research Center (MMRC) at Caltech for optical measurement instruments. Y. T. acknowledges supports from the Sumitomo Foundation (grant no. 120567) and the Murata Science Foundation.

Notes and references

1 L. E. Bell, *Science*, 2008, **321**, 1457–1461.
2 H. Wang, Y. Pei, A. D. LaLonde and G. J. Snyder, *Proc. Natl. Acad. Sci. U. S. A.*, 2012, **109**, 9705–9709.
3 Q. Zhang, H. Wang, W. Liu, H. Wang, B. Yu, Q. Zhang, Z. Tian, G. Ni, S. Lee, K. Esfarjani, G. Chen and Z. Ren, *Energy Environ. Sci.*, 2012, **5**, 5246–5251.
4 J. Androulakis, I. Todorov, J. He, D. Y. Chung, V. Dravid and M. Kanatzidis, *J. Am. Chem. Soc.*, 2011, **133**, 10920–10927.
5 H. Wang, Y. Pei, A. D. Lalonde and G. J. Snyder, *Adv. Mater.*, 2011, **23**, 1366–1370.
6 Q. Zhang, F. Cao, W. Liu, K. Lukas, B. Yu, S. Chen, C. Opeil, D. Broido, G. Chen and Z. Ren, *J. Am. Chem. Soc.*, 2012, **134**, 10031–10038.
7 S. Wang, G. Zheng, T. Luo, X. She, H. Li and X. Tang, *J. Phys. D: Appl. Phys.*, 2011, **44**, 475304.

8 Y. Pei, A. LaLonde, S. Iwanaga and G. J. Snyder, *Energy Environ. Sci.*, 2011, **4**, 2085–2089.
9 A. D. LaLonde, Y. Pei and G. J. Snyder, *Energy Environ. Sci.*, 2011, **4**, 2090–2096.
10 Y. Z. Pei, H. Wang and G. J. Snyder, *Adv. Mater.*, 2012, **24**, 6125–6135.
11 Y. I. Ravich, B. A. Efimova and I. A. Smirnov, *Semiconducting lead chalcogenides*, Plenum Press, New York, 1970.
12 A. Svane, N. Christensen, M. Cardona, A. Chantis, M. van Schilfgaarde and T. Kotani, *Phys. Rev. B: Condens. Matter Mater. Phys.*, 2010, **81**, 245120.
13 D. Parker and D. J. Singh, *Phys. Rev. B: Condens. Matter Mater. Phys.*, 2010, **82**, 035204.
14 D. Parker, D. J. Singh, Q. Zhang and Z. Ren, *J. Appl. Phys.*, 2012, **111**, 123701.
15 H. Wang, A. D. LaLonde, Y. Z. Pei and G. J. Snyder, *Adv. Funct. Mater.*, 2013, **23**, 1586–1596.
16 A. F. Gibson, *Proc. Phys. Soc., London, Sect. B*, 1952, **65**, 378–388.
17 V. A. Saakyan, E. D. Devyatkova and I. A. Smirnov, *Sov. Phys. Solid State*, 1966, **7**, 2541–2542.
18 A. N. Veis, *Sov. Phys. Semiconduct.*, 1982, **16**, 724–725.
19 Y. Pei, X. Shi, A. LaLonde, H. Wang, L. Chen and G. J. Snyder, *Nature*, 2011, **473**, 66–69.
20 W. Liu, X. Tan, K. Yin, H. Liu, X. Tang, J. Shi, Q. Zhang and C. Uher, *Phys. Rev. Lett.*, 2012, **108**, 166601.
21 A. A. Andreev and V. N. Radionov, *Sov. Phys. Semiconduct.*, 1967, **1**, 145–148.
22 N. V. Kolomoets, M. N. Vinogradova and L. M. Sysoeva, *Sov. Phys. Semiconduct.*, 1968, **1**, 1020–1024.
23 C. Jaworski, M. Nielsen, H. Wang, S. Girard, W. Cai, W. Porter, M. Kanatzidis and J. Heremans, *Phys. Rev. B: Condens. Matter Mater. Phys.*, 2013, **87**.
24 Z. M. Gibbs, H. Kim, H. Wang, R. L. White, F. Drymiotis, M. Kaviany and G. J. Snyder, *Appl. Phys. Lett.*, 2014, **104**, DOI: 10.1063/1.4858195.
25 A. N. Veis, R. F. Kuteinikov, S. A. Kumzerov and Y. I. Ukhanov, *Sov. Phys. Semiconduct.*, 1976, **10**, 1320–1321.
26 T. R. Globus and A. O. Olesk, *Sov. Phys. Semiconduct.*, 1985, **19**, 385–388.
27 I. A. Smirnov, B. Y. Moizhes and E. D. Nensberg, *Sov. Phys. Solid State*, 1961, **2**, 1793–1804.
28 M. N. Vinogradova, N. V. Kolomoet, I. M. Rudnik and L. M. Sysoeva, *Sov. Phys. Semiconduct.*, 1969, **3**, 231–232.
29 A. N. Veis, V. I. Kaidanov, R. F. Kuteinikov, S. A. Nemov, S. A. Rudenko and Y. I. Ukhanov, *Sov. Phys. Semiconduct.*, 1978, **12**, 161–163.
30 W. Z. Shen, H. F. Yang, L. F. Jiang, K. Wang, G. Yu, H. Z. Wu and P. J. McCann, *J. Appl. Phys.*, 2002, **91**, 192–198.
31 A. Lambrecht, N. Herres, B. Spanger, S. Kuhn, H. Bottner, M. Tacke and J. Evers, *J. Cryst. Growth*, 1991, **108**, 301–308.
32 A. Majumdar, H. Z. Xu, F. Zhao, J. C. Keay, L. Jayasinghe, S. Khosravani, X. Lu, V. Kelkar and Z. Shi, *J. Appl. Phys.*, 2004, **95**, 939–942.
33 K. Biswas, J. Q. He, Q. C. Zhang, G. Y. Wang, C. Uher, V. P. Dravid and M. G. Kanatzidis, *Nat. Chem.*, 2011, **3**, 160–166.
34 K. Biswas, J. He, I. D. Blum, C. I. Wu, T. P. Hogan, D. N. Seidman, V. P. Dravid and M. G. Kanatzidis, *Nature*, 2012, **489**, 414–418.
35 Y. Lee, S.-H. Lo, J. Androulakis, C.-I. Wu, L.-D. Zhao, D.-Y. Chung, T. P. Hogan, V. P. Dravid and M. G. Kanatzidis, *J. Am. Chem. Soc.*, 2013, **135**, 5152–5160.
36 M. N. Vinogradova, I. M. Rudnik, L. M. Sysoeva and N. V. Kolomoets, *Sov. Phys. Semiconduct.*, 1969, **2**, 892–893.
37 A. N. Veis and Y. I. Ukhanov, *Sov. Phys. Semiconduct.*, 1976, **10**, 780–783.
38 H. Akai, *J. Phys. Soc. Jpn.*, 1982, **51**, 468–474.
39 H. Akai, *J. Phys.: Condens. Matter*, 1989, **1**, 8045–8063.
40 M. Schröter, H. Ebert, H. Akai, P. Entel, E. Hoffmann and G. G. Reddy, *Phys. Rev. B: Condens. Matter Mater. Phys.*, 1995, **52**, 188–209.
41 Y. Takagiwa, Y. Pei, G. Pomrehn and G. Jeffrey Snyder, *APL Mater.*, 2013, **1**, 011101.
42 Y. Takagiwa, Y. Pei, G. Pomrehn and G. J. Snyder, *Appl. Phys. Lett.*, 2012, **101**, 092102.
43 J. P. Heremans, B. Wiendlocha and A. M. Chamoire, *Energy Environ. Sci.*, 2012, **5**, 5510–5530.
44 C. M. Jaworski, B. Wiendlocha, V. Jovovic and J. P. Heremans, *Energy Environ. Sci.*, 2011, **4**, 4155–4162.
45 C. M. Jaworski, J. Tobola, E. M. Levin, K. Schmidt-Rohr and J. P. Heremans, *Phys. Rev. B: Condens. Matter Mater. Phys.*, 2009, **80**, 125208.
46 N. V. Kolomoets, M. N. Vinogradova, E. Y. Lev and L. M. Sysoeva, *Sov. Phys. Solid State*, 1966, **8**, 2925–2928.
47 E. H. Putley, *J. Phys. C: Solid State Phys.*, 1975, **8**, 1837–1840.
48 P. G. Klemens, *Proc. Phys. Soc. London, Sect. A*, 1955, **68**, 1113–1128.
49 P. G. Klemens, *Phys. Rev.*, 1960, **119**, 507–509.
50 B. Abeles, *Phys. Rev.*, 1963, **131**, 1906–1911.
51 J. Yang, G. P. Meisner and L. Chen, *Appl. Phys. Lett.*, 2004, **85**, 1140–1142.
52 H. Wang, A. Charoenphakdee, K. Kurosaki, S. Yamanaka and G. J. Snyder, *Phys. Rev. B: Condens. Matter Mater. Phys.*, 2011, **83**, 024303.
53 J. Callaway and H. C. Vonbaeyer, *Phys. Rev.*, 1960, **120**, 1149–1154.
54 J. W. Harrison and J. R. Hauser, *Phys. Rev. B: Condens. Matter Mater. Phys.*, 1976, **13**, 5347–5350.
55 J. R. Hauser, M. A. Littlejohn and T. H. Glisson, *Appl. Phys. Lett.*, 1976, **28**, 458–461.
56 L. Makowski and M. Glicksman, *J. Phys. Chem. Solids*, 1973, **34**, 487–492.
57 K. Y. Tsou and E. B. Hensley, *J. Appl. Phys.*, 1974, **45**, 47–49.
58 I. B. S. Banu, M. Rajagopalan, B. Palanivel, G. Kalpana and P. Shenbagaraman, *J. Low Temp. Phys.*, 1998, **112**, 211–226.
59 D. Rached, M. Rabah, N. Benkhettou, B. Soudini and H. Abid, *Phys. Status Solidi B*, 2004, **241**, 2529–2537.
60 R. Graham and D. Yu, *Nano Lett.*, 2012, **12**, 4360–4365.
61 S.-H. Wei and A. Zunger, *Phys. Rev. B: Condens. Matter Mater. Phys.*, 1997, **55**, 13605–13610.
62 Y. Z. Pei, A. D. LaLonde, N. A. Heinz, X. Y. Shi, S. Iwanaga, H. Wang, L. D. Chen and G. J. Snyder, *Adv. Mater.*, 2011, **23**, 5674–5678.

63 L. D. Zhao, H. J. Wu, S. Q. Hao, C. I. Wu, X. Y. Zhao, K. Biswas, J. Q. He, T. P. Hogan, C. Uher, C. Wolverton, V. P. Dravid and M. G. Kanatzidis, *Energy Environ. Sci.*, 2013, **6**, 3346–3355.
64 Z. M. Gibbs, A. D. LaLonde and G. J. Snyder, *New J. Phys.*, 2013, **15**, 075020.
65 U. V. Barth and L. Hedin, *J. Phys. C: Solid State Phys.*, 1972, **5**, 1629.
66 K. A. Borup, E. S. Toberer, L. D. Zoltan, G. Nakatsukasa, M. Errico, J. P. Fleurial, B. B. Iversen and G. J. Snyder, *Rev. Sci. Instrum.*, 2012, **83**, 123902.
67 S. Iwanaga, E. S. Toberer, A. Lalonde and G. J. Snyder, *Rev. Sci. Instrum.*, 2011, **82**, 063905.
68 R. Blachnik and R. Igel, *Z. Naturforsch., B: Anorg. Chem., Org. Chem.*, 1974, **29**, 625–629.